

Review

Ground energy balance for borehole heat exchangers: Vertical fluxes, groundwater and storage



Jaime A. Rivera ^{a,*}, Philipp Blum ^b, Peter Bayer ^a

^a ETH Zürich, Department of Earth Sciences, Sonneggstrasse 5, 8092 Zurich, Switzerland

^b Karlsruhe Institute of Technology (KIT), Institute for Applied Geosciences (AGW), Kaiserstraße 12, 76131 Karlsruhe, Germany

ARTICLE INFO

Article history:

Received 13 January 2015

Received in revised form

22 May 2015

Accepted 26 May 2015

Available online 23 June 2015

Keywords:

Geothermal energy

Heat transport

Sources of power

System recovery

ABSTRACT

Borehole heat exchangers (BHE) are the most frequent applications for extracting low-enthalpy geothermal energy. Their effect on shallow ground is commonly assessed by modeling the in-situ thermal conditions with little attention on the transient heat flux regime stimulated by BHEs. Here, we characterize these heat fluxes using analytical models. The approach is applied to a field site with long-term monitoring of the ground temperature development around a BHE. Our major findings are that advective transport shapes vertical heat fluxes and the power provided to the system from groundwater and from storage substantially varies over time. Examination of power sources reveals that during early operation phase, energy is extracted mainly from the storage. Then, local depletion enhances the vertical fluxes with the relative contribution from the bottom reaching a limit of 24% of the total power demand, whereas that from the ground surface becomes dominant for $Fo > 0.13$. Long-term energetic analysis, including the time after system shutdown, highlights that recovery may take much longer than the operation time. However, axial heat fluxes accelerate recovery and the ground surface then becomes even more dominant providing about two thirds of the power over the full life-cycle of the studied standard system.

© 2015 Elsevier Ltd. All rights reserved.

1. Introduction

The consumption of low-enthalpy energy for heating and cooling has led to accelerated depletion of fossil fuels and is a main contributor to the carbon footprint of countries. In search of alternative and preferably renewable energies, the shallow ground has evolved as an increasingly popular source, which has a great advantage: it is directly accessible and available everywhere. Worldwide, the capacity of shallow geothermal applications is rising, and only in the European Union, geothermal heat pumps provided around 1400 ktoe (16 Mio. MWh) in 2011, with estimated greenhouse gas (GHG) emissions savings of around 4 Mio. tons CO₂ [1,2]. The most common variants of geothermal heat pumps utilize vertical boreholes of 50–400 m depth, with installed plastic tubes that exchange energy with the ground. These borehole heat exchangers (BHEs) are well-controlled closed systems without mass transfer, where energy is exchanged by pumping a carrier fluid through the plastic tubes loops [3].

With the huge number of installed BHEs, meanwhile technical design follows routine recipes [4,5]. For each case, BHE numbers, configurations and individual lengths are oriented at the energy demand, expected lifetime, ground properties and performance of the heat pump [6–8]. Still, routine practices bear the risk of neglecting opportunities in case-specific system design, dynamic control and fine-tuning [9,10]. This was for example demonstrated for multiple BHE fields, with improved performance potential through optimization of individual BHEs operation mode and position [11,12]. A crucial point in standard planning is that the heat transport processes in the ground are often roughly approximated, assuming uniform heat conduction only. This may lead to the misconception that extracted shallow geothermal energy originates exclusively from the ground and is supplied by conduction from the earth's interior only. However, for instance, neglecting top boundary effects, disregards typically pronounced thermal gradients at the ground surface [13]. These gradients delineate potentially relevant thermal fluxes towards a BHE. If they are not accounted for, this may lead to inaccurate system design and wrong estimations of the magnitude of the induced thermal anomalies [14,15]. As another process, heat advection by groundwater can play a substantial role. It shapes thermal plumes and can potentially

* Corresponding author.

E-mail address: jaime.rivera@erdw.ethz.ch (J.A. Rivera).

Nomenclature	
a	thermal diffusivity ($\text{m}^2 \text{s}^{-1}$)
c	volumetric heat capacity of porous medium ($\text{MJ m}^{-3} \text{K}^{-1}$)
Fo	Fourier number
f	vertical heat flux distribution (W m^{-2})
F	dimensionless form of f
G	Green's function
H	borehole length (m)
n_e	effective porous medium porosity
p	power (W)
P	dimensionless form of p
Pe	Péclet number
q_d	Darcy velocity (m y^{-1})
q	heat flow rate per unit length (W m^{-1})
r_h	horizontal radial distance from the borehole (m)
R	dimensionless form of r_h
t	time (s)
T	temperature in the porous medium ($^{\circ}\text{C}$)
T_o	reference temperature ($^{\circ}\text{C}$)
v	effective thermal velocity (m s^{-1})
\mathbf{x}	coordinates vector where temperature is evaluated (m)
\mathbf{x}'	coordinates vector where a heat source is released (m)
x, y, z	single space coordinates where temperature is evaluated (m)
x', y', z'	single space coordinates where heat sources are released (m)
X, Y, Z	dimensionless form of x, y, z
<i>Greek symbols</i>	
λ	thermal conductivity of porous medium ($\text{W m}^{-1} \text{K}^{-1}$)
τ	time at which a heat pulse is released (s)
φ, φ_H	intermediate or substitution variables
<i>Subscripts</i>	
w	wetting phase
s	solid phase
<i>Abbreviations</i>	
BHE	borehole heat exchanger
CV	control volume
CS	control surface in the CV
FLS	finite line source
GSF	groundwater flow
GSHP	ground source heat pump
MFLS	moving finite line source

replenish generated ground energy deficits [16–18]. Altogether, the relevant contributors to the energy sourced from the ground and their respective shares in the energy balance are defined by site-specific conditions. These shares, however, have not yet been analyzed in detail. Our objective is to shed light on these geothermal energy sources and their time-dependent contributions. By quantification of heat fluxes and power supply, we understand how the different physical mechanisms interact, and ultimately can provide fundamental criteria for balanced and hence sustainable BHE operation.

Sustainability is in fact an issue that spans the entire lifetime of ground source heat pump (GSHP) systems. This lifetime typically comprises decades when extraction and injection of heat is rarely balanced [13,19]. This could be achieved for instance by optimized seasonal operation or by combining heat extraction with heat injection [20–22]. Given an imbalance, thermal anomalies in the ground often grow over the years. As they potentially entail a decline in a geothermal system's performance, pronounced thermal anomalies are not desirable. Aside from this, induced thermal disturbances of the ground and groundwater are frequently restricted, to minimize environmental impacts and to give equal prospects to neighboring applications [23,24]. In some studies, long-term operation as well as ground recovery time after hypothetical shutdown of the system was examined. Ungemacht et al. [25] and Rybach et al. [26] estimated that the (approximated) initial thermal state can be reached after a time span similar to the operation period. This regeneration time span, however, is sensitive to the system size (single or multiple BHEs), configuration and specific site conditions [27,28]. After the shut-down, the rate of regeneration is fastest, driven by pronounced thermal gradients. At later times, this rate declines while the temperature around the BHE asymptotically approaches the initial state. Thus, judging regeneration based on the evolution of ground temperature is plausible, but it does not give direct insight in the replenishment of the bulk ground energy deficit.

Since long-term field measurements are rare, models serve as key tools for predicting the ground thermal evolution around BHEs. A broad range of different variants exists, from fast temperature

response functions (g-functions) and exact, but simplifying analytical models, to demanding numerical models [29–35]. In this work, we set up an analytical modeling framework, which is customarily based on Kelvin's line source theory for prediction of in-situ ground temperatures. However, in our study, we do not focus on the temperature. Rather, and this is original, we examine the heat fluxes stimulated by long-term BHE operation for heat extraction. This includes basal fluxes, those from the ground surface and by reservoir depletion.

By utilizing a versatile analytical model framework, general and specific findings can be obtained. For example, it is feasible to characterize the influence of groundwater flow on the spatial and temporal distribution of vertical heat fluxes. Despite the fact that many previous studies have pointed out the positive influence of groundwater flow on BHEs performance [18,36–39], it is unclear under which conditions advection enhances vertical fluxes. Our model framework allows quantifying heat fluxes at the top boundary and borehole toe. Furthermore, by direct integration of these fluxes over their thermally influenced area, simple closed analytical equations can be obtained for the associated power supply. With these, an overall ground energy balance is performed. This is important, firstly, to highlight the relevance of considered heat flux processes and, secondly, because it represents an efficient tool to analyze the long-term ground temperature behavior during BHE operation and subsequent recovery from a power-supply perspective.

In the following, we first present the analytical tools for estimating vertical heat fluxes and total power at the top boundary and the BHE toe based on an alternative form of the moving finite line source [40]. Then, a dimensional analysis is performed to describe the spatial and temporal dynamics of these fluxes while changing variables such as groundwater flow and heat exchanger length. This is fundamental for the subsequent analysis of the temporal evolution of the dimensionless power from different sources. The presented models are also applied to the previously studied Elgg site [41,42], where long-term temperature data is available and analytical models have successfully been validated [15]. Finally, a simulation of the power dynamics after hypothetical BHE shut-down is presented.

2. Methodology

A schematic representation of the energy balanced during a BHE operation is depicted in Fig. 1. In the shown cylindrical control volume (CV) the total power extracted qH is supplied by induced vertical heat fluxes at the top boundary, bottom plane as well as thermal exhaustion of the medium around the BHE.

For the control volume, heat fluxes exist across the control surface (CS). For the sake of generality, the radius of the CV is considered infinite, thus the CS reduces to the top and bottom planes. Accordingly, three sources of energy or power can be identified: the top boundary ($p(z=0,t)$), the bottom plane ($p(z=H,t)$) and the stored/extracted heat ($p(0 < z < H,t)$) within the CV. The total power balance can be written as

$$p(z=0,t) + p(z=H,t) + p(0 < z < H,t) = qH \quad (1)$$

The BHE is approximated here as a finite line source (FLS) [34,43]. This approximation enables the use of (semi-)analytical expressions that solve the conduction-advection transport problem [44,45]. Despite the fact that these expressions are restricted to semi-infinite homogeneous and fully saturated porous media with steady and uniform horizontal groundwater flow, they are widely accepted due to their versatility and considerably lower computational cost when compared with existing numerical methods (e.g. [36]). Additionally, these models are suitable for studying long-term effects [46], which are of special interest in our analysis of the ground energy balance during and after the life cycle of a BHE. The FLS model incorporates heat exchange with the atmosphere through a top boundary with constant temperature. There exist alternative analytical models that relax this assumption based on the principle of superposition [14,15]. However, since our focus here is the heat balance exclusively associated with the BHE operation, the self-balanced FLS model is favored.

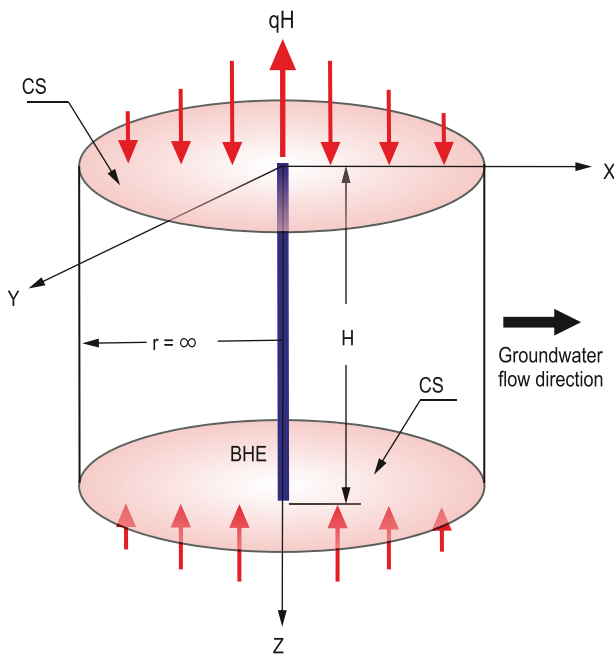


Fig. 1. Cylindrical control volume (CV) for heat balance calculation. Red arrows indicate heat fluxes, and qH is the total power extracted by the BHE. CS denotes the control surface of the CV. (For interpretation of the references to colour in this figure legend, the reader is referred to the web version of this article.)

Computation of heat fluxes is essential for quantifying the ground energy balance. The standard formulation of the moving FLS model (MFLS) [40] is not suitable to determine vertical fluxes. We implement an alternative formulation of the MFLS that facilitates direct heat flux calculation and the estimation of the total power resulting from the integration of these fluxes over their area of influence. The standard MFLS comprises two superposition effects in this order: the first one applied to continuous heat sources in time with constant strength (qdz') and located at a given fixed position (x', y', z'). The second one accounts for the same heat source distributed along the borehole ($z' \in [0, H]$). By inverting this superpositioning order, the alternative formulation is obtained [14,47,48].

We start with the Green's function for a unitary instantaneous heat source in a semi-infinite domain [44]:

$$G(\mathbf{x}, \mathbf{x}', t - \tau) = \frac{1}{8[\pi a(t - \tau)]^{3/2}} \exp\left(-\frac{r_h^2}{4a(t - \tau)}\right) \times \left\{ \exp\left[-\frac{(z - z')^2}{4a(t - \tau)}\right] - \exp\left[-\frac{(z + z')^2}{4a(t - \tau)}\right] \right\}, \quad z \geq 0 \quad (2)$$

where $r_h^2 = (x - x')^2 + (y - y')^2$. Eq. (2) yields the temperature at (x, y, z, t) due to a unitary pulse released at (x', y', z', τ) , while keeping zero temperature at the top boundary. If, instead of a unitary pulse, a continuous and finite line source (length H) is considered, the temperature at (x, y, z, t) is obtained via integration of Eq. (2) as follows:

$$T(r_h, z, t) - T_o = \frac{q}{8c(\pi a)^{3/2}} \int_0^t \frac{1}{(t - \tau)^{3/2}} \exp\left(-\frac{r_h^2}{4a(t - \tau)}\right) \int_0^H \left\{ \exp\left[-\frac{(z - z')^2}{4a(t - \tau)}\right] - \exp\left[-\frac{(z + z')^2}{4a(t - \tau)}\right] \right\} dz' d\tau \quad (3)$$

where T_o is any reference (or initial) temperature. Eq. (3) can be reorganized so that the inner integral over z' is evaluated first. This yields [47]:

$$T(r_h, z, t) - T_o = \frac{q}{8\lambda\pi} \int_0^t \frac{1}{(t - \tau)} \exp\left(-\frac{r_h^2}{4a(t - \tau)}\right) \times \left[2\operatorname{erf}\left(\frac{z}{2\sqrt{a(t - \tau)}}\right) - \operatorname{erf}\left(\frac{z - H}{2\sqrt{a(t - \tau)}}\right) - \operatorname{erf}\left(\frac{z + H}{2\sqrt{a(t - \tau)}}\right) \right] d\tau \quad (4)$$

Uniform and steady groundwater flow along the x direction can be incorporated via the moving source method [44]. By substituting x with $x - v(t - \tau)$, Eq. (4) becomes:

$$T(r_h, z, t) - T_o = \frac{q}{8\lambda\pi} \int_0^t \frac{1}{(t-\tau)} \exp \left[-\frac{(x-\nu(t-\tau)-x')^2 + (y-y')^2}{4a(t-\tau)} \right] \left\{ 2\operatorname{erf} \left(\frac{z}{2\sqrt{a(t-\tau)}} \right) - \operatorname{erf} \left(\frac{z-H}{2\sqrt{a(t-\tau)}} \right) - \operatorname{erf} \left(\frac{z+H}{2\sqrt{a(t-\tau)}} \right) \right\} d\tau \tag{5}$$

With the substitution $\varphi = \frac{r_h^2}{4a(t-\tau)}$, we obtain a more compacted form for Eq. (5):

$$T(r_h, z, t) - T_o = \frac{q}{8\lambda\pi} \exp \left(\frac{x-x'}{2a}\nu \right) \int_{\frac{r_h^2}{4at}}^{\infty} \frac{1}{\varphi} \exp \left[-\varphi - \left(\frac{r_h\nu}{4a} \right) \frac{21}{\varphi} \right] \left\{ 2\operatorname{erf} \left(\frac{z}{r_h\sqrt{\varphi}} \right) - \operatorname{erf} \left(\frac{z-H}{r_h\sqrt{\varphi}} \right) - \operatorname{erf} \left(\frac{z+H}{r_h\sqrt{\varphi}} \right) \right\} d\varphi \tag{6}$$

This formulation is more efficient in terms of computational cost (around 30% less time of computation) and more convenient for calculating the vertical heat fluxes at the top ($z = 0$) and bottom ($z = H$) planes shown in Fig. 1. The analytical expressions for these fluxes are indicated in Eqs. (7) and (8), respectively.

$$f(r_h, z=0, t) = \lambda \frac{\partial T}{\partial z} \Big|_{z=0} = \frac{q}{2r_h\pi^{3/2}} \exp \left(\frac{x-x'}{2a}\nu \right) \int_{\frac{r_h^2}{4at}}^{\infty} \frac{1}{\sqrt{\varphi}} \exp \left(-\varphi - \left(\frac{r_h\nu}{4a} \right) \frac{21}{\varphi} \right) \left[1 - \exp \left(-\frac{H^2\varphi}{r_h^2} \right) \right] d\varphi \tag{7}$$

$$f(r_h, z=H, t) = -\lambda \frac{\partial T}{\partial z} \Big|_{z=H} = -\frac{q}{4r_h\pi^{3/2}} \exp \left(\frac{x-x'}{2a}\nu \right) \int_{\frac{r_h^2}{4at}}^{\infty} \frac{1}{\sqrt{\varphi}} \exp \left(-\varphi - \left(\frac{r_h\nu}{4a} \right) \frac{21}{\varphi} \right) \times \left[2\exp \left(-\frac{H^2\varphi}{r_h^2} \right) - \exp \left(-\frac{4H^2\varphi}{r_h^2} \right) - 1 \right] d\varphi \tag{8}$$

In Eqs. (7) and (8) positive heat fluxes values indicate heat inflow into the CV. Their dimensionless forms are:

$$F(R, Z=0, Fo, Pe) = \frac{2r_h\pi^{3/2}}{q} f(r_h, z=0, t) = \exp \left(\frac{X}{2}Pe \right) \int_{\frac{R^2}{4Fo}}^{\infty} \frac{1}{\sqrt{\varphi}} \exp \left(-\varphi - \left(\frac{PeR}{4} \right) \frac{21}{\varphi} \right) \times \left[1 - \exp \left(-\frac{\varphi}{R^2} \right) \right] d\varphi \tag{9}$$

$$F(R, Z=H, Fo, Pe) = \frac{2r_h\pi^{3/2}}{q} f(r_h, z=H, t) = -\frac{1}{2} \exp \left(\frac{X}{2}Pe \right) \int_{\frac{R^2}{4Fo}}^{\infty} \frac{1}{\sqrt{\varphi}} \exp \left(-\varphi - \left(\frac{PeR}{4} \right) \frac{21}{\varphi} \right) \left[2\exp \left(-\frac{\varphi}{R^2} \right) - \exp \left(-\frac{4\varphi}{R^2} \right) - 1 \right] d\varphi \tag{10}$$

where $Pe = \frac{vH}{\alpha}$ is the Péclet number with $\nu = \frac{qa_c w}{c}$, $Fo = \frac{at}{H^2}$ is the Fourier number and $R = \frac{r_h}{H}$, $X = \frac{x-x'}{H}$.

The total power is an interesting metric for estimating the energy contribution from the top boundary and the bottom plane. For the top boundary, for instance, the total power is obtained by integrating Eq. (7) over its influential area A (plane $z = 0$):

$$p(z=0, t) = \int_A \mathbf{f}(r_h, z=0, t) \cdot d\mathbf{A} = \int_{-\infty}^{\infty} \int_{-\infty}^{\infty} f(r_h, z=0, t) dx dy \tag{11}$$

Eq. (11) is in reality a triple integral whose solution is computationally expensive. When we calculate the fluxes $f(r_h, z=0, \tau)$ with Eq. (5), we get an analogous expression as a function of x and y (instead of φ):

$$p(z=0, t) = \int_{-\infty}^{\infty} \int_{-\infty}^{\infty} f(x, y, z=0, \tau) dx dy = \frac{q}{4\sqrt{a}\pi^3} \int_0^t \int_{-\infty}^{\infty} \int_{-\infty}^{\infty} \frac{1}{(t-\tau)^{3/2}} \exp \left(-\frac{(x-\nu(t-\tau)-x')^2 + (y-y')^2}{4a(t-\tau)} \right) \left[1 - \exp \left(-\frac{H^2}{4a(t-\tau)} \right) \right] dx dy d\tau \tag{12}$$

Grouping the variables in Eq. (12) gives

$$p(z=0, t) = \frac{q}{4\sqrt{a}\pi^3} \int_0^t \frac{1}{(t-\tau)^{3/2}} \left[1 - \exp \left(-\frac{H^2}{4a(t-\tau)} \right) \right] \times \left\{ \int_{-\infty}^{\infty} \exp \left[-\frac{(x-\nu(t-\tau)-x')^2}{4a(t-\tau)} \right] dx \int_{-\infty}^{\infty} \exp \left[-\frac{(y-y')^2}{4a(t-\tau)} \right] dy \right\} d\tau \tag{13}$$

The two improper inner integrals (over x and y) are the same regardless of the value of ν , since τ is a constant in this ambit. In other words, for the integral over x , the effective thermal velocity ν only shifts the integrand in a magnitude $\nu(t-\tau)$, but the area below the integrand remains equal to the integral over y . The latter, in turn, is simply the normalization factor for a Gaussian distribution, and then:

$$\int_{-\infty}^{\infty} \exp\left[-\frac{(x-v(t-\tau)-x')^2}{4a(t-\tau)}\right] dx \int_{-\infty}^{\infty} \exp\left[-\frac{(y-y')^2}{4a(t-\tau)}\right] dy = \left[2\sqrt{\pi a(t-\tau)}\right]^2 \tag{14}$$

Substituting Eq. (14) in Eq. (13) yields:

$$p(z=0, t) = q\sqrt{\frac{a}{\pi}} \int_0^t \frac{1}{(t-\tau)^{1/2}} \left[1 - \exp\left(-\frac{H^2}{4a(t-\tau)}\right)\right] d\tau \tag{15}$$

At this point the triple integral in Eq. (12) has been reduced to a single integral over τ . This integral can be further simplified. With the change of variable $\phi_H = \frac{H^2}{4a(t-\tau)}$, Eq. (15) thus is rewritten as:

$$p(z=0, t) = \frac{qH}{2\sqrt{\pi}} \int_{\frac{H^2}{4at}}^{\infty} \frac{1}{\phi_H^{3/2}} [1 - \exp(-\phi_H)] d\phi_H \tag{16}$$

Splitting the integral in Eq. (16), both integrands can be evaluated analytically as follows:

$$p(z=0, t) = \frac{qH}{2\sqrt{\pi}} \left[\int_{\frac{H^2}{4at}}^{\infty} \frac{d\phi_H}{\phi_H^{3/2}} - \int_{\frac{H^2}{4at}}^{\infty} \frac{\exp(-\phi_H)}{\phi_H^{3/2}} d\phi_H \right] = \frac{qH}{2\sqrt{\pi}} \left[-\frac{2}{\sqrt{\phi_H}} - 2\sqrt{\pi} \operatorname{erf}(-\sqrt{\phi_H}) + \frac{2}{\sqrt{\phi_H}} \exp(-\phi_H) \right]_{\frac{H^2}{4at}}^{\infty} \tag{17}$$

Finally, by evaluating the integration limits, the total power at the top boundary is obtained:

$$p(z=0, t) = qH \left[\sqrt{\frac{4at}{\pi H^2}} + \operatorname{erf}\left(-\frac{H}{\sqrt{4at}}\right) - \sqrt{\frac{4at}{\pi H^2}} \exp\left(-\frac{H^2}{4at}\right) + 1 \right] \tag{18}$$

A similar procedure can be done for the vertical fluxes and total power supply at the bottom plane. This yields:

$$p(z=H, t) = \int_A \mathbf{f}(r_h, z=H, t) \cdot d\mathbf{A} = \int_{-\infty}^{\infty} \int_{-\infty}^{\infty} f(r_h, z=H, t) dx dy = qH \left\{ \operatorname{erf}\left(-\frac{H}{\sqrt{at}}\right) - \operatorname{erf}\left(-\frac{H}{\sqrt{4at}}\right) + \sqrt{\frac{at}{\pi H^2}} \left[2\exp\left(-\frac{H^2}{4at}\right) - \exp\left(-\frac{H^2}{at}\right) - 1 \right] \right\} \tag{19}$$

The corresponding dimensionless forms of the total power for both planes can be written as:

$$P(Z=0, Fo) = \frac{p(z=0, t)}{qH} = \sqrt{\frac{4Fo}{\pi}} + \operatorname{erf}\left(-\frac{1}{\sqrt{4Fo}}\right) - \sqrt{\frac{4Fo}{\pi}} \exp\left(-\frac{1}{4Fo}\right) + 1 \tag{20}$$

$$P(Z=1, Fo) = \frac{p(z=H, t)}{qH} = \operatorname{erf}\left(-\frac{1}{\sqrt{Fo}}\right) - \operatorname{erf}\left(-\frac{1}{\sqrt{4Fo}}\right) + \sqrt{\frac{Fo}{\pi}} \left[2\exp\left(-\frac{1}{4Fo}\right) - \exp\left(-\frac{1}{Fo}\right) - 1 \right] \tag{21}$$

Eqs. 18–21 and Eqs. 7–10 are the basis for the temporal and spatial description of ground heat fluxes and power supply in the next chapter. This is complemented by applying the methodology to the well-documented Elgg field site [41,42].

3. Results and discussion

3.1. Heat fluxes

The BHE shown in Fig. 1 is our synthetic case study. It is assumed to be installed in sandy homogeneous aquifer with the following typical properties [13]: effective porosity $n_e = 0.2$, bulk thermal conductivity $\lambda = 2.1 \text{ W m}^{-1} \text{ K}^{-1}$, volumetric heat capacity of water $c_w = 4.2 \text{ MJ K}^{-1} \text{ m}^{-3}$ and of solids $c_s = 2.20 \text{ MJ K}^{-1} \text{ m}^{-3}$. The corresponding bulk properties of the porous medium are calculated following a porosity-weighted arithmetic mean [13]. Finally, it is assumed that the BHE has a length (H) of 50 m and it extracts energy at a rate $q = 40 \text{ W m}^{-1}$. At this stage of our analysis, this rather short length is chosen in order to focus primarily on the role of the top boundary, and longer BHEs will be studied subsequently.

Through Eqs. 7–10 heat flux distributions can be obtained along the axes longitudinal (absolute x or dimensionless X) and transversal (absolute y or dimensionless Y) to horizontal groundwater flow. Fig. 2 illustrates a distribution of vertical fluxes at the top boundary in dimensionless (Fig. 2a) and absolute (Fig. 2b) magnitudes. In the simulation, Darcy flux is kept constant at $q_d = 9.4 \text{ m y}^{-1}$ (or $Pe = 30$), which corresponds to a groundwater seepage velocity of 47 m y^{-1} . These are typical values for sandy aquifers [46]. The shown fluxes are calculated after 10 years of operation ($Fo = 0.1$). The strong deformation of the absolute fluxes when plotted in unitless quantities is due to the factor $\frac{1}{l_h}$ in Eq. (7), which increases the fluxes close to the BHE. Comparing the fluxes in Fig. 2b with common values of the natural geothermal flux ($60\text{--}80 \text{ mW/m}^{-2}$ [49,50]) for instance, higher magnitudes are seen along the x direction within a horizontal distance of $x = 78 \text{ m}$ downstream of the BHE.

A more general characterization of heat fluxes and associated power requires the use of the dimensionless groups identified in the Methodology section (Chap. 2) with borehole length (H) taken as the characteristic length. This means that if the same thermal diffusivity of our synthetic case is kept, a $Fo = 0.1$ for instance, is equivalent to 10 or 39 years of operation for $H = 50 \text{ m}$ or $H = 100 \text{ m}$ respectively. Similarly, a $Pe = 60$ corresponds to Darcy fluxes of $q_d = 18.8 \text{ m y}^{-1}$ for $H = 50 \text{ m}$ or $q_d = 9.4 \text{ m y}^{-1}$ for $H = 100 \text{ m}$. These dimensionless numbers generally indicate what the drivers of the heat flux distributions are and how different processes are compared based on the parameters of the physical model.

Fig. 3 depicts the influence of groundwater flow on the vertical heat flux distribution at the top boundary ($Z = 0$). The shown fluxes are calculated for different Pe numbers while keeping constant $Fo = 0.1$. According to the figure, groundwater flow leads to an asymmetric deformation of the heat flux field with a maximum value at the borehole location where a model singularity exists. Fig. 3a represents a cross sectional view along the groundwater flow direction, where advection enhances heat input in the downstream side while notoriously decreases it upstream. In

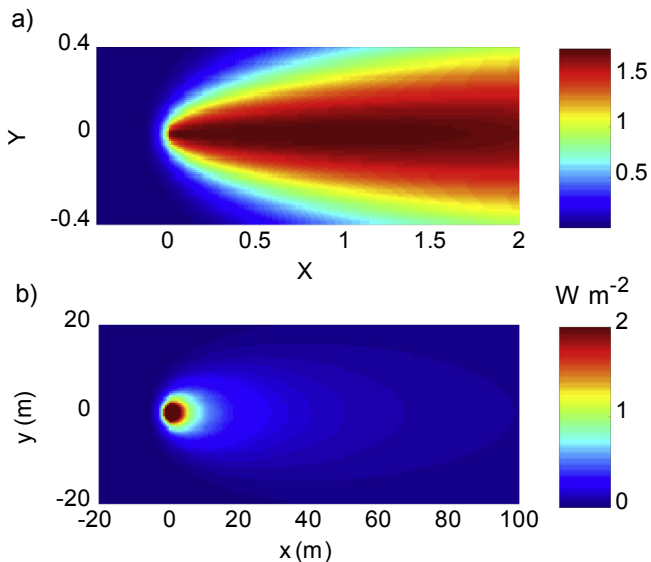


Fig. 2. Vertical heat fluxes at the top boundary at: $t = 10$ years ($Fo = 0.1$), $q_d = 9.4 \text{ m y}^{-1}$ ($Pe = 30$); (a) dimensionless magnitudes according to Eq. (9), and (b) absolute values (W m^{-2}) according to Eq. (7). Groundwater flows along the x direction, borehole length $H = 50 \text{ m}$, $q = 40 \text{ W m}^{-1}$. BHE is located at $(0,0)$.

contrast, in the perpendicular profile of Fig. 3b, the distribution keeps its symmetry, but the moving water washes out the diffusive fluxes yielding systematically lower fluxes for higher Pe values.

The physical interpretation of the flux distribution shown in Fig. 3a is strongly linked to the prescribed temperature at the top boundary. This condition attenuates the effect of the advective heat transport on the temperature distribution close to the boundary (e.g. [15]) and, at the same time, leads to more pronounced vertical gradients. Consequently, the more extended a thermal plume is (i.e. higher Pe number for a fixed time), the higher the estimated vertical fluxes along the flow direction. This is one reason why the curves associated with higher Pe numbers in Fig. 3a tend to be flattened in their upstream part expanding the maximum heat flux downstream.

Comparing the fluxes in X and Y directions reveals a compensation in the heat flux distribution. Higher fluxes downstream are compensated with lesser heat input upstream and in transversal direction. This is in fact corroborated by Eq. (18), where the total power supplied through the top boundary is independent of the effective thermal velocity, v . Hence, in spite of the deformation of the vertical heat flux fields induced by groundwater flow, the power supplied through both considered horizontal planes is the same as for conduction-dominated conditions. At this point it is important to recall that the moving line source model (MFLS) is suited for scenarios without heat input from lateral boundaries and thus, arriving groundwater flow is thermally unaffected (same temperature as the ambient far-field). Moreover, the moving point source method is an artefact to include advective transport under the assumption that the bulk porous medium is moving (solid matrix and groundwater). In such cases, advection transports the instantaneous heat fluxes induced by the BHE operation and advancing thermal plumes delineate the domain where reservoir exhaustion takes place. Since the extracted energy rate (qH in Fig. 1) is independent of the velocity v , the overall power balance (Eq. (1)) is also unaffected by groundwater flow. In a real system however, the drawdown of temperature in the solid matrix around the borehole creates thermal gradients that stimulate net heat influx from advection ($q_d c_w \frac{\partial T}{\partial x}$). With the described line source model it

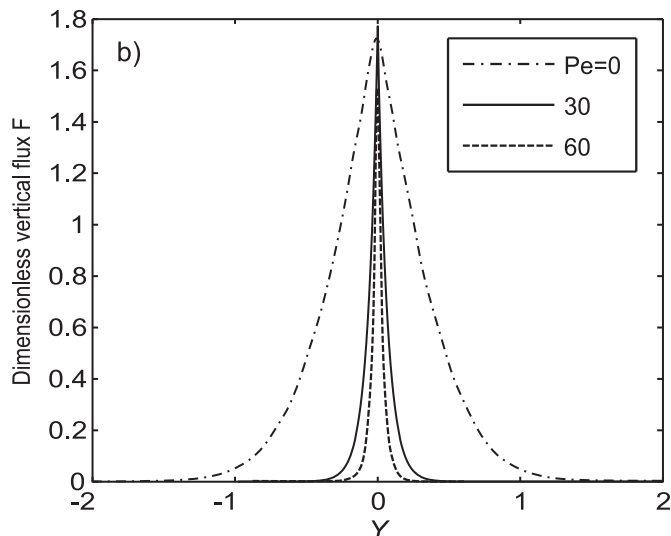
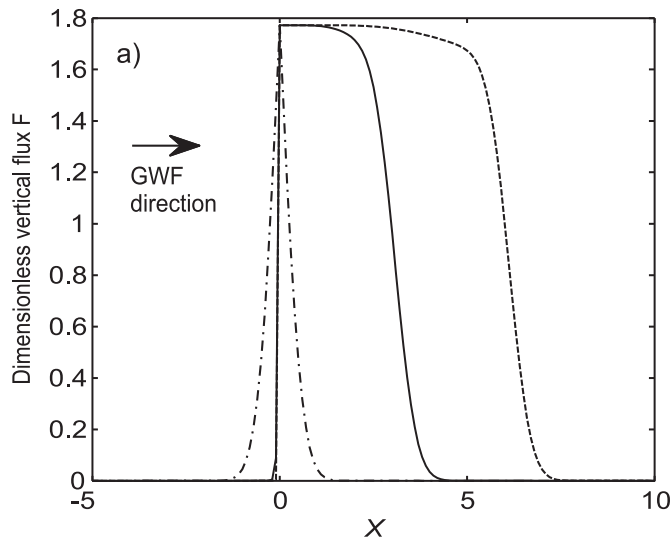


Fig. 3. Vertical heat fluxes along X (a) and Y (b) direction at the plane $Z = 0$ (Fig. 1). Pe numbers are tuned by changing the Darcy flux, other parameters are fixed. The BHE is located at $(0,0)$. GWF: groundwater flow.

is not possible to differentiate the power contribution from these two sources, i.e. groundwater and reservoir exhaustion. Thus, it is assumed that the effect of a “moving porous medium” is equivalent to the energy replenishing the reservoir by groundwater flow.

Besides groundwater flow, borehole length is another parameter included in the dimensionless groups that has a potential impact on the vertical fluxes at the top boundary. Fig. 4 shows these fluxes for three different H values. In this analysis, Darcy flux is kept at $q_d = 9.4 \text{ m y}^{-1}$ and the time of evaluation is $t = 10$ years. The results indicate that in both axes, a considerably lower heat contribution from the top boundary is expected for longer BHEs. By comparing Figs. 3 and 4, it can also be concluded that the compensation effect is not present here, because in this dimensionless form, Pe only varies due to the different H (in Fig. 3 the differences are due to q_d). This relative lower heat input implies that other sources of energy become more relevant for longer BHEs.

The other plane of interest is the bottom plane of the CV ($z = H$ or $Z = 1$). Fig. 5 depicts the vertical heat fluxes distribution along the two main axes while changing the Darcy flux, q_d . When comparing with the fluxes from top in Fig. 3, the magnitudes here

are around half due to the continuity of the medium at the BHE toe. The fluxes in the Y direction (Fig. 5b) keep their symmetry, again, with lower values under higher Pe . The compensation effect for the heat flux distribution is therefore also present here, in line with the insensitivity of Eq. (21) to the Pe number.

The borehole length H also affects the heat fluxes at the bottom plane in a similar way as that indicated in Fig. 4 for the top boundary (figure not shown here). The observed lower heat fluxes for longer BHEs, in both horizontal planes and in both axes, indicate that thermal depletion around the borehole is more relevant in the energy balance.

Fig. 6 illustrates the behavior of the vertical fluxes at the top boundary in dimensionless time (Fo number). In Fig. 6a, the reference $Pe = 30$ is fixed while three different points located at the same distance from the BHE (upstream, downstream and perpendicular to groundwater flow direction) are chosen. Clearly, the position has a strong influence in the computed steady-state flux. The lowest fluxes correspond to the point located upstream of the BHE (stronger compensation effect under groundwater flow). In Fig. 6b, the effect of different Pe numbers over time is analyzed. Similar to previous studies focused on the role of groundwater flow on steady-state temperatures (e.g. [15,40]), vertical heat fluxes

reach a steady state faster under higher effective thermal velocities.

At the bottom plane, the fluxes at enough distance from the BHE and after a certain time are downward directed (heat outflow from the CV), as shown in Fig. 7. This figure is analogous to Fig. 5a, but the curves here correspond to different dimensionless times (Fo); the Péclet number is fixed at $Pe = 30$. The domain affected by the downward heat fluxes seems to increase with time. This is a consequence of the prescribed temperature at the ground surface. After a certain time, the influence of the latter reaches the borehole toe and downward fluxes can overcome the upward ones induced by the BHE operation. However, this can only be seen in regions distant enough from the borehole where the BHE influence is weaker.

3.2. Ground power balance

The total power supplied by both horizontal planes is calculated as the integral over the entire plane of the inner product between the corresponding vertical heat flux field and the differential area (Eq. (11) and (19)). Fig. 8 illustrates the dimensionless magnitudes as a function of the Fo number. Since the total extracted power is set to the unity in this unitless plot, the figure also indicates the share

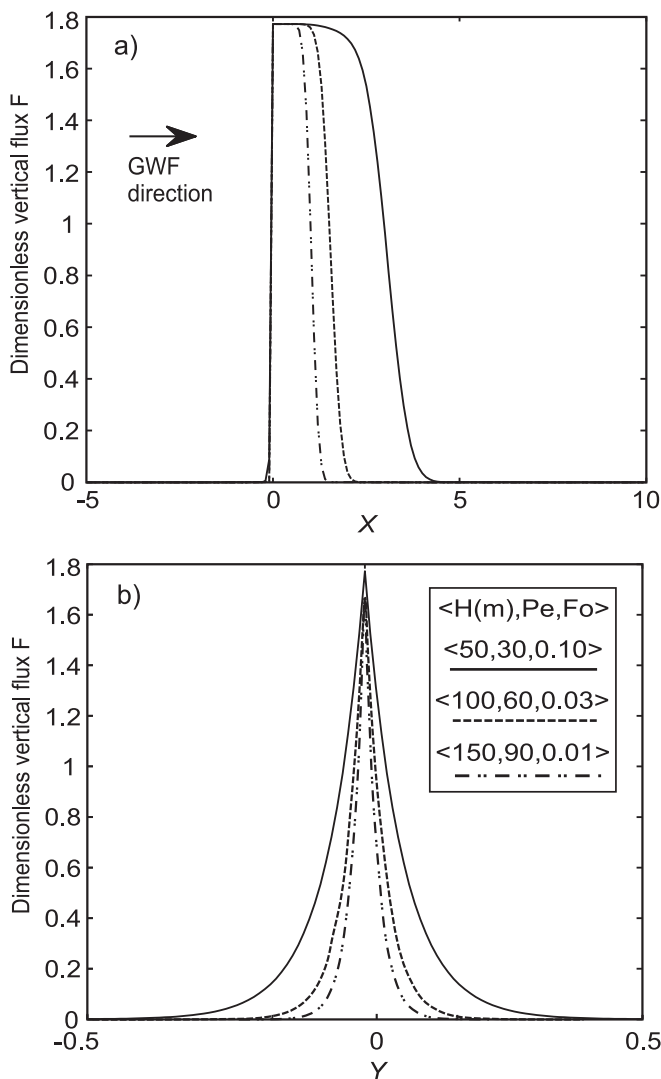


Fig. 4. Vertical heat fluxes along X (a) and Y (b) direction at the plane $Z = 0$ (see Fig. 1). Pe and Fo are tuned by changing H , other parameters are fixed. The BHE is located at the origin $(0,0)$. GWF: groundwater flow.

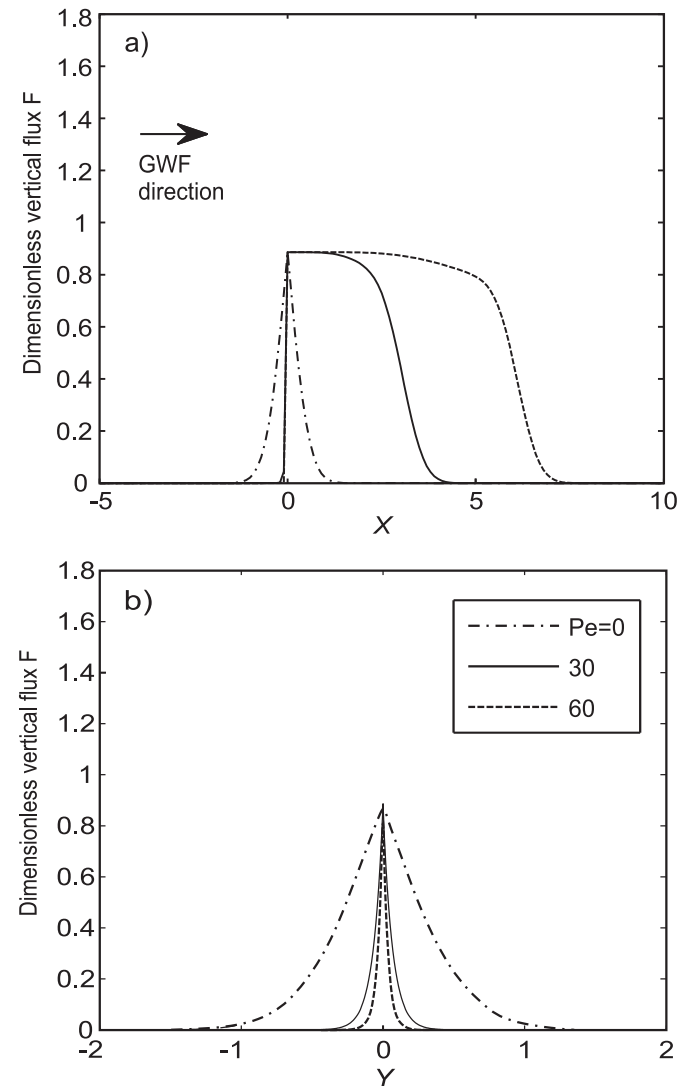


Fig. 5. Vertical heat fluxes along X (a) and Y (b) direction at the plane $Z = H$ (see Fig. 1). Pe numbers are tuned by changing the Darcy flux, other parameters are fixed. The BHE is located at $(0,0)$. GWF: groundwater flow.

of each energy source for supplying the entire power demand.

For the porous medium considered in our synthetic model, a $Fo = 0.1$ corresponds to around 39 years of operation for a BHE with $H = 100$ m. After this rather long period, the contribution from the bottom plane reaches approximately 18% while the power from top supplies up to 35% of the demand. To fulfill the entire heat extraction rate, the missing percentage is supplied by heat exhaustion of the medium around the BHE (47%). The latter source is crucial from the beginning of the operation until $Fo \approx 0.13$. It is also more determinant for longer BHEs associated with lower Fo numbers when time is fixed.

In the long run (i.e. when $t \rightarrow \infty$), the dimensionless power from top (Eq. (20)) approaches the unity meaning that the entire power demand is supplied by fluxes from the ground surface. Conversely, Eq. (21) tends to zero in the same limit implying that, for $Fo \approx 0.41$, the contribution from the bottom plane reaches a maximum ($P \approx 0.24$) as shown in Fig. 8. This condition however, is not reached for BHE lengths exceeding 50 m if practical life times of these systems are considered (no more than 40 years of operation). Taking $H = 50$ m for instance, the maximum contribution from the

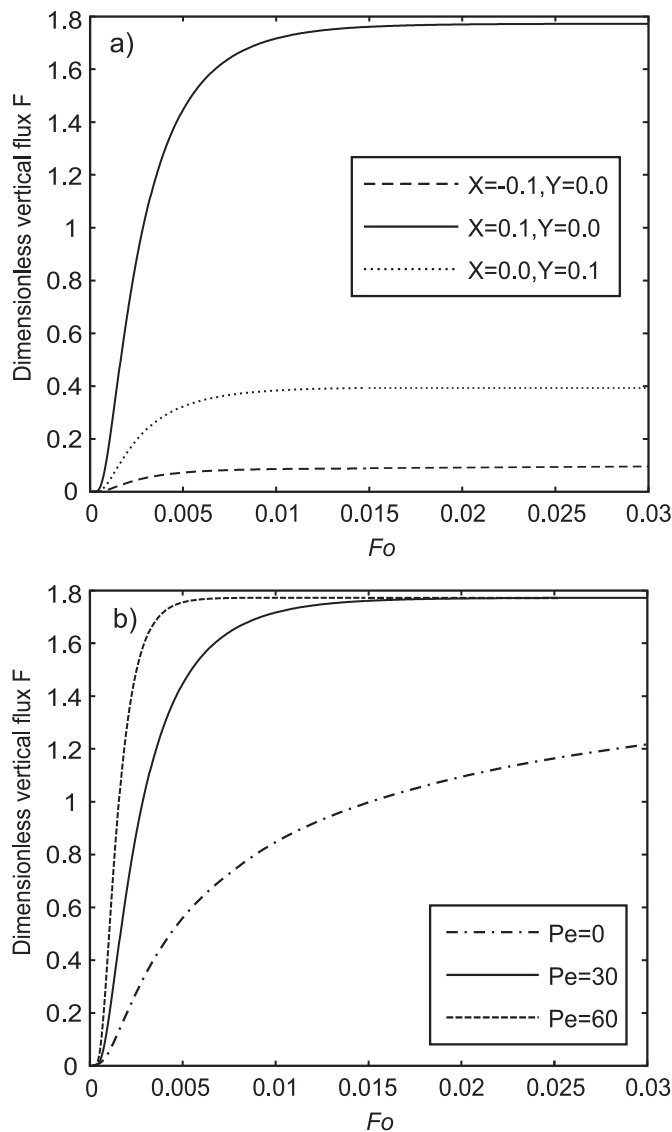


Fig. 6. Vertical heat fluxes in time at $Z = 0$ for (a) different X and Y locations and fixed $Pe = 30$. (b) different Pe (here changing the Darcy flux) and fixed position $X = 0.1, Y = 0$.

bottom plane is expected after 40 years of operation. In any case, the continuous decrease of the power supply after this time does not imply that the heat flux distribution also approaches zero at the bottom plane. As shown in Fig. 7, a high heat flux input is seen close to the BHE toe, but in areas far enough an inversion of the vertical fluxes is expected. These two effects counteract each other in the long term, leading to a systematic decrease of the net power at the bottom plane.

3.3. Application to the Elgg field site

A single coaxial vertical ground source heat pump (GSHP) system with 105 m length and a heat extraction rate of up of 70 W m^{-1} has been installed in a single house in the rural area of the municipality of Elgg close to Zurich, Switzerland. Several measurement campaigns have been carried out where depth-dependent ground temperatures were recorded. The site and the characteristics of the installed GSHP are described in Eugster [41].

Rivera et al. [15] simulated the temporal and spatial distribution of the thermal anomaly induced by the system using analytical solutions. The BHE was approximated as a finite line source with unbalanced heat extraction rate. The satisfactory results obtained in this study case allow the use of the presented analytical expressions to study the contributors of power in a real system. In accordance with Rivera et al. [15], the variable load was incorporated within the MFLS via temporal superposition of a stepwise function representing the transient rate. Thus, the vertical heat fluxes and the total power supply can be calculated as

$$f'(r_h, z, t) = \sum_{i=1}^N f(q^i - q^{i-1}, r_h, z, t^N - t^i), \quad z = 0, H \quad (22)$$

$$p'(z, t) = \sum_{i=1}^N p(z, t^N - t^i), \quad z = 0, H \quad (23)$$

where N is the number of months and the functions f and p are defined in Eqs. (7), (8), (18) and (19).

Fig. 9 shows these magnitudes for the top and bottom planes during the first 12 years of operation. The increasing power supply

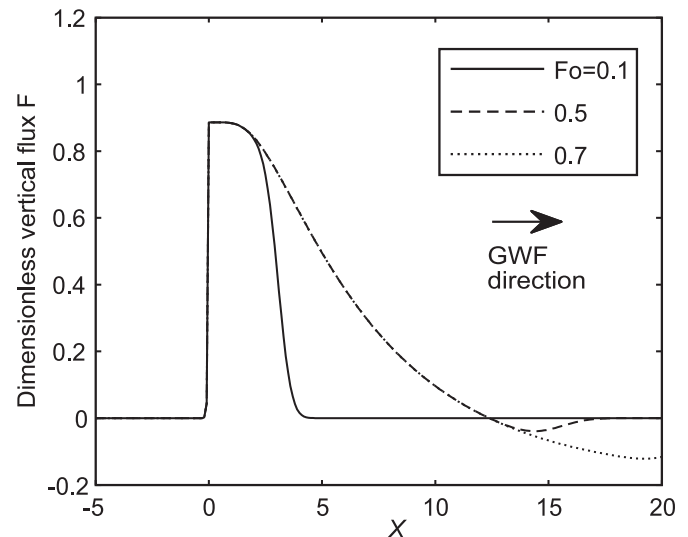


Fig. 7. Vertical heat fluxes along X direction at the plane $Z = H$ (see Fig. 1) and $Pe = 30$. Fo numbers are tuned by changing the time, other parameters are fixed. The BHE is located at the origin $(0,0)$. GWF: groundwater flow.

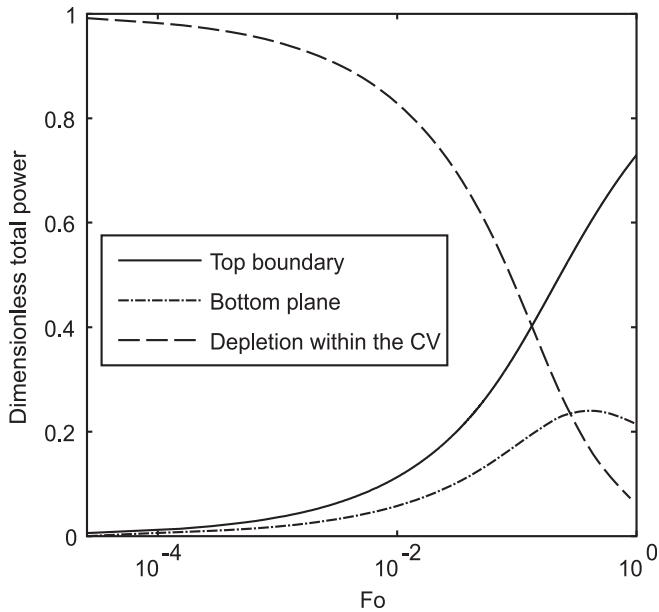


Fig. 8. Dimensionless total power supply from reservoir depletion within the CV and the top and bottom planes in dimensionless time (Fo in logarithmic scale).

from both horizontal planes is a consequence of a more intensive and more expanded thermal anomaly induced by the BHE operation. Rybach and Eugster [42] obtained heat flux as much as 3 W m^{-2} close to the BHE at 105 m depth and during the heating period of the eleventh year from numerical simulations. Using the analytical expressions, similar magnitudes are found at 0.4 m distance from the BHE toe (at the same time).

Fig. 10 illustrates the overall power balance at the site. Neglecting the seasonal variations and taking the annual power mean in Fig. 9, Fig. 10b indicates the share of the total power demand provided by the top and bottom planes. As can be seen, after 12 years the top boundary contributes around 23% of the demand whereas the bottom plane contributes approximately 12%. The missing 65% is supplied by reservoir depletion around the BHE.

The medium and long-term performance of the BHE at this site has been extensively studied. Signorelli et al. [27] and Eugster and Rybach [51] for instance, used numerical simulations and field measurements to demonstrate that, after an initially strong temperature drop, the system reaches a sustainable operation level after 12 years. This level is characterized by a stabilized maximum drop of 1–2 K in the temperature-depth-profile measured in an observation well located 1 m distant from the BHE. In contrast, we are able to study this observation with the total power supplied by reservoir depletion in the same time window. Taking $t=12$ years, $H=105$ m and a thermal diffusivity of $a=1.3 \times 10^{-6} \text{ m}^2 \text{ s}^{-1}$ [15]; the calculated Fourier number is $Fo = 0.05$. With this value as input, Fig. 8 indicates that the system is far from being in a quasi-equilibrium. This agrees with our expectation where (quasi-) steady power states occur in a different time scale since energy, contrary to temperature, is an extensive (and aggregated) property in the system. Nevertheless, such Fourier number almost coincides with the one at which the highest rate of reservoir recovery is expected (inflection point in the power supply curve from the reservoir in Fig. 8).

A related analysis on how the power sources react after a hypothetical shutdown of the system can be addressed with the proposed analytical framework. If the shutdown occurs at $t = t^*$, the total power input from both planes can be calculated as

$$\begin{aligned} p'(z, t) &= p(z, t), & 0 \leq t < t^*, & \quad z = 0, H \\ p'(z, t) &= p(z, t) - p(z, t - t^*), & t^* < t \leq \infty, & \quad z = 0, H \end{aligned} \quad (24)$$

where the function p is as given in Eqs. (18) and (19). Taking the mean annual heat extraction rate and assuming $t^* = 30$ years, Fig. 11 shows the power input in time. As can be seen, in terms of power, the recovery period is much longer than the one of production. Rybach et al. [26] and Rybach and Eugster [52] estimated a similar time for these two periods using numerical models but focused on the change of temperature at a fixed position. However, changes in local temperature are lower in time when the heat extraction rate is kept constant (or in a quasi-steady state). This is due the higher input from the top boundary and the increasing thermally affected volume around the BHE.

Fig. 11 indicates that the thermal recovery is faster at the BHE toe due to the continuity of the porous medium. At the end of the 30th year, heat fluxes at both planes provide around 900 W out of the demanded 1666 W. Afterwards, the storage around the BHE is replenished at a rate equal to the sum of the power supply from both planes (Eq. (1) with $q = 0$). The top boundary becomes the main contributor to the storage recovery since its heat input remains higher during the entire time window. Immediately after the shutdown, this boundary retrieves around 60% of the current reservoir gain, whereas after 60 years of recovery period it contributes with approximately 80%.

4. Conclusions

When simulating the impacts of borehole heat exchangers (BHEs) we commonly focus on the temperature evolution in the ground, which is fundamental for the extraction capacity, the temperature in the heat carrier fluid and the entire performance of the system. Also regulative constraints are typically formulated based on temperature thresholds, such as maximum allowed ground or groundwater cooling. Local temperatures alone, however, give little insight in the induced ground heat flux regime. We cannot discriminate original energy sources, and this may lead to a

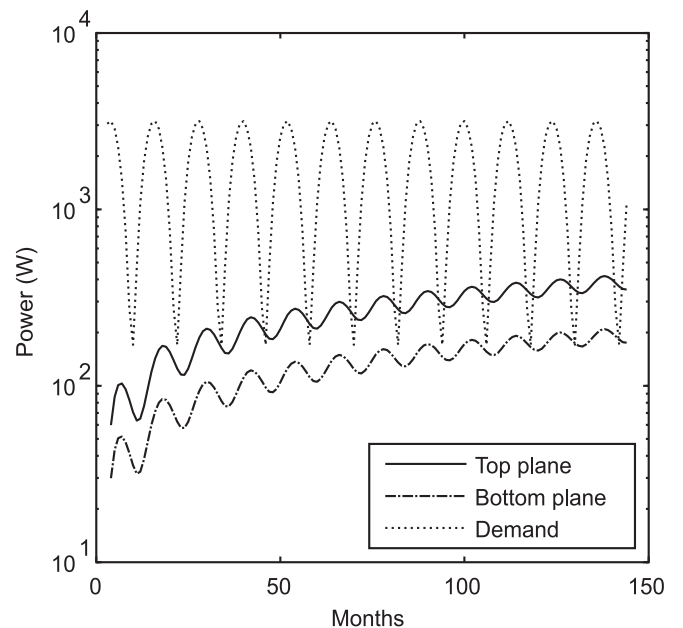


Fig. 9. Power demand and power supply from the top and bottom planes for the BHE installed at the Elgg site. The heat extraction rate and the porous medium properties are taken from Rivera et al. [15].

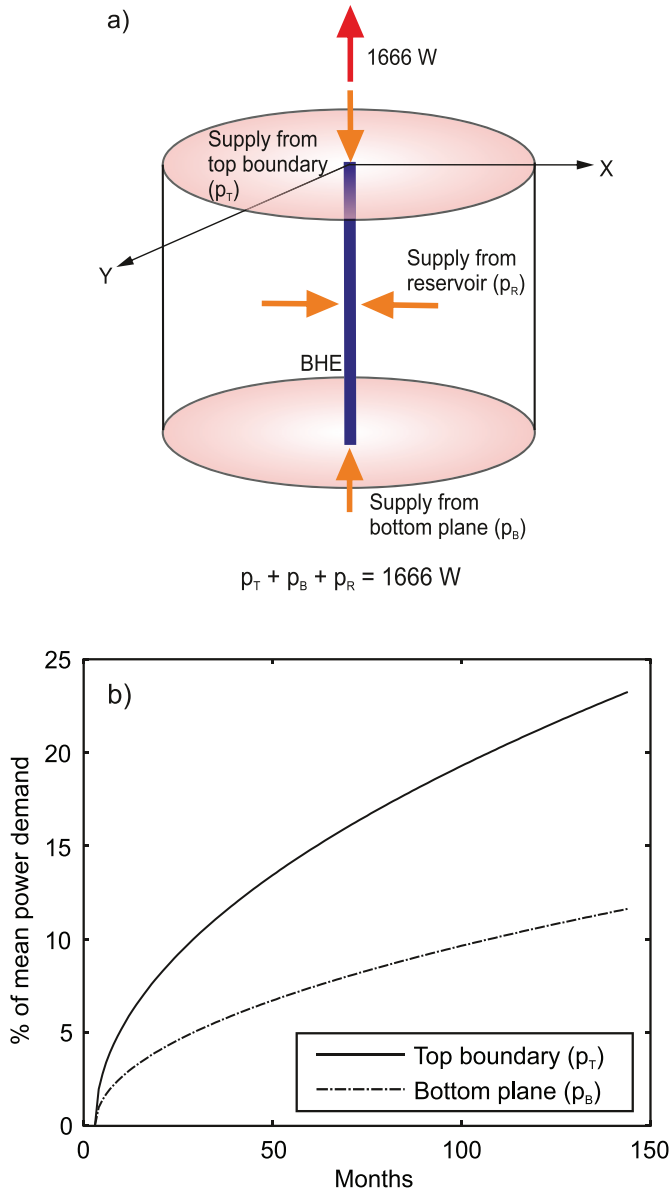


Fig. 10. Power balance for the BHE installed at the Elgg site; (a) scheme identifying the heat sources and (b) fractions of the total power demand (%) supplied by the top (p_T) and bottom planes (p_B). p_R is the power contribution from the reservoir. The annual mean power demand is 1666 W.

wrong and simplified picture, where all energy mined from the ground comes from the earth interior. In our analysis, we implemented analytical line source equations in order to quantify the bulk vertical and lateral heat fluxes and for distinction of the basic power contributors. As a reference, a cylindrical control volume is defined. The presented dimensionless analysis together with the field case application facilitates general conclusions, which are fundamental for judgment of the sustainability and renewability of shallow geothermal applications.

In a first step, we examined the interplay of borehole length and groundwater seepage velocity for long-term evolution of heat fluxes towards a typical BHE installed in a sandy aquifer. In general, heat fluxes from the ground surface are the double of those estimated at the basal plane. It is also shown how increasing horizontal advection (expressed by higher Peclet numbers) enhances vertical conductive heat flux in the downstream in both horizontal planes. However, with the moving line source simulation, we cannot

separate power contribution from storage and flowing groundwater, and the bulk vertical power contributions remain the same. The second focus is on the ground power balance and the original sources of energy. Dimensionless analysis shows that at early stages energy is extracted mainly from the storage. However, this contribution declines with time transferring the leading role to the ground surface for $Fo > 0.13$. At the basal plane, it is estimated that its power contribution reaches a limit of around 24% of the total power demand at $Fo \approx 0.41$. A premise for this is that the line source equation assuming a uniform specific heat extraction rate is valid. With increasing depth the temperature in the ground typically rises, which in reality elevates the heat extraction rate. This is not accounted for, and accordingly our approach is an approximation. Thus, even though line source equations are standardized tools for simulating BHEs of several hundreds of meters length, the error induced for the energy balance may not be acceptable for very deep BHEs.

For a BHE of 100 m, even after several decades, the energetic source is mainly the reservoir exhaustion whereas the ground surface supplies up to 35% of the demanded power. However, when the heat fluxes after system shutdown are included in the analysis, the vertical heat fluxes replenish the reservoir. With this more comprehensive life cycle perspective, the origin of shallow geothermal energy is by two thirds from the atmosphere, and one third from the earth's interior. This means, the main source of shallow geothermal energy ultimately is not the ground, independent of the length of the borehole.

The presented framework also offers different metrics for geothermal sustainability. Commonly, local temperature measurements around a BHE are used to judge recovery progress and time. The focus on bulk energy deficit in the ground, and its evolution during and after system operation, offers a more rigorous analysis. It is revealed that in absence of groundwater flow, the declining thermal gradients around the borehole decelerate recovery on the long run. For the typical field case selected in our study, after the same time of recovery as of operation, only 55% of the energy deficit is replenished. It is also shown that the vertical heat fluxes are crucial for this analysis and their neglect would yield wrong

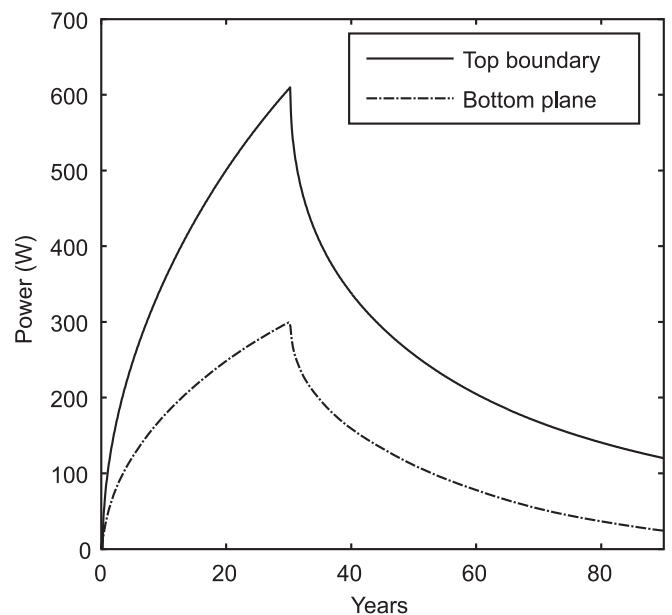


Fig. 11. Annual mean power supply from the top and bottom planes for the BHE installed at the Elgg site assuming a permanent shutdown of the system after 30 years of operation.

predictions. By including these contributors, however, a holistic, three dimensional energetic assessment is facilitated, which offers a new perspective for judging renewability and sustainability of low-enthalpy geothermal technologies.

Acknowledgments

We thank two reviewers for their constructive comments. This work was supported by the Swiss National Science Foundation (SNSF) under grant number 200021L 144288, and the German Research Foundation (DFG), under grant number BL 1015/4-1, and, within the GEOTHERM-II project, by the Competence Center Energy and Mobility (CCEM) and Competence Center for Environment and Sustainability (CCES) of the ETH-Domain. We thank Gabi Moser for language corrections.

References

- [1] P. Bayer, et al., Greenhouse gas emission savings of ground source heat pump systems in Europe: a review, *Renew. Sustain. Energy Rev.* 16 (2) (2012) 1256–1267.
- [2] EurObserv'ER, The state of renewable energies in Europe, in: 13th EurObserv'ER Report, 2013 (Paris), www.energies-renouvelables.org.
- [3] G. Florides, S. Kalogirou, Ground heat exchangers—a review of systems, models and applications, *Renew. Energy* 32 (15) (2007) 2461–2478.
- [4] J. Spittler, M. Bernier, Ground-source heat pump systems: the first century and beyond, *HVAC&R Res.* 17 (6) (2011) 891–894.
- [5] S.P. Kavanaugh, K.D. Rafferty, *Ground-source Heat Pumps: Design of Geothermal Systems for Commercial and Institutional Buildings*, American Society of Heating, Refrigerating and Air-Conditioning Engineers, 1997.
- [6] S. Dehkordi, R. Schincariol, Guidelines and the design approach for vertical geothermal heat pump systems: current status and perspective, *Can. Geotechnical J.* 51 (999) (2014) 1–16.
- [7] VDI, *Thermische Nutzung des Untergrundes (Guideline for thermal use of the underground)*, in: Vdi-richtlinie 4640, Verein Deutscher Ingenieure (VDI)-Gesellschaft Energietechnik, Germany, 2012.
- [8] MCS, *Microgeneration Installation Standard (MIS): 3005, Issue 3.0 in Micro-generation Certification Scheme (MCS)*, Department of Energy and Climate Change (DECC), London, 2011.
- [9] H. Madani, J. Claesson, P. Lundqvist, Capacity control in ground source heat pump systems: part I: modeling and simulation, *Int. J. Refrig.* 34 (6) (2011) 1338–1347.
- [10] H. Cho, J.M. Choi, The quantitative evaluation of design parameter's effects on a ground source heat pump system, *Renew. Energy* 65 (2014) 2–6.
- [11] M. Beck, et al., Geometric arrangement and operation mode adjustment in low-enthalpy geothermal borehole fields for heating, *Energy* 49 (2013) 434–443.
- [12] M. de Paly, et al., Optimization of energy extraction for closed shallow geothermal systems using linear programming, *Geothermics* 43 (2012) 57–65.
- [13] F. Stauffer, et al., *Thermal Use of Shallow Groundwater*, CRC Press, 2013.
- [14] T. Bandos, et al., Finite line-source model for borehole heat exchangers: effect of vertical temperature variations, *Geothermics* 38 (2) (2009) 263–270.
- [15] J.A. Rivera, P. Blum, P. Bayer, Analytical simulation of groundwater flow and land surface effects on thermal plumes of borehole heat exchangers, *Appl. Energy* 146 (0) (2015) 421–433.
- [16] A. García-Gil, et al., The thermal consequences of river-level variations in an urban groundwater body highly affected by groundwater heat pumps, *Sci. Total Environ.* 485–486 (0) (2014) 575–587.
- [17] J.C. Choi, J. Park, S.-R. Lee, Numerical evaluation of the effects of groundwater flow on borehole heat exchanger arrays, *Renew. Energy* 52 (2013) 230–240.
- [18] A. Casasso, R. Sethi, Efficiency of closed loop geothermal heat pumps: a sensitivity analysis, *Renew. Energy* 62 (2014) 737–746.
- [19] J. Chen, et al., An experimental investigation on ground heat flow balance issue for a GCHP, *Int. J. Low-Carbon Technol.* 6 (1) (2011) 70–75.
- [20] E.C. Kang, et al., New approach to evaluate the seasonal performance of building integrated geothermal heat pump system, *Renew. Energy* 54 (2013) 51–54.
- [21] P. Bayer, M. de Paly, M. Beck, Strategic optimization of borehole heat exchanger field for seasonal geothermal heating and cooling, *Appl. Energy* 136 (2014) 445–453.
- [22] G. Florides, et al., Geothermal properties of the ground in cyprus and their effect on the efficiency of ground coupled heat pumps, *Renew. Energy* 49 (2013) 85–89.
- [23] S. Haehnlein, P. Bayer, P. Blum, International legal status of the use of shallow geothermal energy, *Renew. Sustain. Energy Rev.* 14 (9) (2010) 2611–2625.
- [24] S. Hahnlein, et al., Sustainability and policy for the thermal use of shallow geothermal energy, *Energy Policy* 59 (2013) 914–925.
- [25] P. Ungemach, M. Papachristou, M. Antics, Renewability versus sustainability. A reservoir management approach, in: *Proceedings of the European Geothermal Congress*, 2007.
- [26] L. Rybach, T. Mège, W. Eugster, At what time scale are geothermal resources renewable, in: *Proceedings of World Geothermal Congress 2000*, 2000.
- [27] S. Signorelli, T. Kohl, L. Rybach, Sustainability of production from borehole heat exchanger fields, in: *29th Workshop on Geothermal Reservoir Engineering*, 2004.
- [28] S. Erol, M.A. Hashemi, B. François, Analytical solution of discontinuous heat extraction for sustainability and recovery aspects of borehole heat exchangers, *Int. J. Therm. Sci.* 88 (2015) 47–58.
- [29] M. Alalaimi, et al., Effect of size on ground-coupled heat pump performance, *Int. J. Heat Mass Transf.* 64 (2013) 115–121.
- [30] G. Florides, P. Christodoulides, P. Pouloupatis, An analysis of heat flow through a borehole heat exchanger validated model, *Appl. Energy* 92 (2012) 523–533.
- [31] M. Li, et al., Full-scale temperature response function (G-function) for heat transfer by borehole ground heat exchangers (GHEs) from sub-hour to decades, *Appl. Energy* 136 (2014) 197–205.
- [32] Z. Li, A new constant heat flux model for vertical U-tube ground heat exchangers, *Energy Build.* 45 (2012) 311–316.
- [33] D. Mottaghy, L. Dijkshoorn, Implementing an effective finite difference formulation for borehole heat exchangers into a heat and mass transport code, *Renew. Energy* 45 (2012) 59–71.
- [34] H. Zeng, N. Diao, Z. Fang, A finite line-source model for boreholes in geothermal heat exchangers, *Heat Transfer—Asian Res.* 31 (7) (2002) 558–567.
- [35] J.M. Choi, et al., Numerical simulation for thermal response test performance in closed-loop vertical ground heat exchanger, *Sci. China Technol. Sci.* 54 (7) (2011) 1668–1673.
- [36] D. Banks, A review of the importance of regional groundwater advection for ground heat exchange, *Environ. Earth Sci.* (2014) 1–11.
- [37] A. Angelotti, et al., Energy performance and thermal impact of a borehole heat exchanger in a sandy aquifer: influence of the groundwater velocity, *Energy Convers. Manag.* 77 (2014) 700–708.
- [38] A.D. Chiasson, S.J. Rees, J.D. Spittler, a preliminary assessment of the effects of ground-water flow on closed-loop ground-source heat pump systems, *ASHRAE Trans.* 106 (1) (2000) 380–393.
- [39] W. Zhang, et al., The analysis on solid cylindrical heat source model of foundation pile ground heat exchangers with groundwater flow, *Energy* 55 (2013) 417–425.
- [40] N. Molina-Giraldo, et al., A moving finite line source model to simulate borehole heat exchangers with groundwater advection, *Int. J. Therm. Sci.* 50 (12) (2011) 2506–2513.
- [41] W. Eugster, *Erdwärmesonden-Funktionsweise und Wechselwirkung mit dem geologischen Untergrund*, 1991. Diss. Naturwiss. ETH Zürich, Nr. 9524, 1991.
- [42] L. Rybach, W. Eugster, Sustainability aspects of geothermal heat pump operation, with experience from Switzerland, *Geothermics* 39 (4) (2010) 365–369.
- [43] P. Eskilson, *Thermal analysis of Heat Extraction Boreholes*, Ph.D. Thesis, University of Lund, Lund, Sweden, 1987.
- [44] H. Carslaw, J. Jaeger, *Conduction of Heat in Solids*, second ed., Oxford University Press, New York, 1959.
- [45] N. Diao, Q. Li, Z. Fang, An analytical solution of the temperature response in geothermal heat exchangers with groundwater advection [J], *J. Shandong Inst. Archit. Eng.* 3 (2003) 000.
- [46] M. Tye-Gingras, L. Gosselin, Generic ground response functions for ground exchangers in the presence of groundwater flow, *Renew. Energy* 72 (2014) 354–366.
- [47] J. Claesson, S. Javed, An analytical method to calculate borehole fluid temperatures for time-scales from minutes to decades, *ASHRAE Trans.* 117 (2) (2011) 279–288.
- [48] Y. Man, et al., A new model and analytical solutions for borehole and pile ground heat exchangers, *Int. J. Heat Mass Transf.* 53 (13) (2010) 2593–2601.
- [49] S. Gruber, et al., Interpretation of geothermal profiles perturbed by topography: the Alpine permafrost boreholes at Stockhorn Plateau, Switzerland, *Permafrost. Periglacial Process.* 15 (4) (2004) 349–357.
- [50] V. Wagner, et al., Numerical sensitivity study of thermal response tests, *Renew. Energy* 41 (2012) 245–253.
- [51] W. Eugster, L. Rybach, Sustainable production from borehole heat exchanger systems, in: *Proceedings World Geothermal Congress*, 2000.
- [52] L. Rybach, W. Eugster, Sustainability aspects of geothermal heat pumps, in: *27th Workshop on Geothermal Reservoir Engineering*, 2002.